Preparation and properties of SiO_2–SiO_x heterostructures formed by uninterrupted processing by remote plasma enhanced chemical vapor deposition

D. V. Tsu, S. S. Kim, J. A. Theil, Cheng Wang, and G. Lucovsky
Departments of Physics, and Materials Science and Engineering, North Carolina State University, Raleigh, North Carolina 27695-8202

(Received 20 November 1989; accepted 29 January 1990)

Heterostructures of SiO_2 and SiO_x are formed by remote plasma enhanced chemical vapor deposition without switching or interrupting the gases and their flow through the deposition chamber, or the radio-frequency (rf) power. Selectively exciting the process gases, e.g., only oxygen (O_2) or both O_2 and silane (SiH_4) simultaneously, produces SiO_2 or SiO_x, respectively. Only when the plasma afterglow extends into the chamber, thereby activating silane, do suboxides form. Control of the plasma afterglow is accomplished with the plasma bias assembly, located between the plasma tube and the deposition region, and heterostructures are formed by switching the grid bias between floating and grounded states. We have examined the deposited heterostructures by transmission electron microscopy (TEM) and find the oxide/suboxide transition is abrupt. Electrical properties of the suboxide layers in metal/SiO_2/Sio_1/SiO_2/n-Si structures have been investigated by C–V measurements. Three different structures, having oxide thicknesses of ~20, 40, and 84 Å deposited onto the c-Si substrate have been investigated; the suboxide layer is 150 Å and the second oxide is fixed at 165 Å. Application of a + 5 V gate bias allows electrons to tunnel through the 20 and 40 Å oxides into the suboxide, but the 84 Å oxide prevents any tunnel injection. The electrical characteristics of the metal/SiO_2/SiO_1/SiO_2/n-Si structures are controlled by the tunneling of electrons into, and out of the suboxide layers.

I. INTRODUCTION

The deposition of many different thin film materials is often required in the fabrication of modern electronic devices, and to deposit these different materials often requires different atomic sources and/or deposition methods. This usually necessitates the transfer of the sample from one system, optimized for the formation of one of the layers, to another. In the context of plasma enhanced chemical vapor deposition (PECVD), different materials are usually deposited by using different source gases, and sometimes different regimes of pressure, radio-frequency (rf) power, etc. The manufacture of multilayer heterostructures in a single chamber may involve switching on and off the flow the various process gases, with particular attention to the residence time of each of the process gases in the chamber, and the time required to deposit one monolayer of material.[1,2] Formation of multilayer structures may also involve rotating the deposition surface between chambers in order to provide sequential exposure to different process gases.[3]

We show in this paper, by taking advantage of different deposition *chemistries*, multilayer heterostructures of silicon dioxide (SiO_2) and silicon suboxides (SiO_x) can be produced by remote PECVD[4] in a continuous fashion *without* altering any of the process variables, i.e., the particular process gases, their flow rates, the rf power, the substrate temperature, or the deposition pressure. Deposition selectivity is obtained by controlling the bias state of a grid which can be used to control the extraction of charged species out of the plasma generation region. The underlying principle in changing the chemical constitution of the deposited then involves the ability to selectively excite the downstream injected process gases by controlling charged particle injection into the deposition region. This can be represented schematically by considering two reactant gases, A and B, which are injected downstream from a plasma excitation region. When gas A is activated, the deposition reaction is

$$A^* + B \rightarrow \text{film } \alpha\,, \tag{1}$$

where the star indicates activation by species extracted from the plasma, and film α is deposited. On the other hand, if gas B is also activated, by changing the state of bias on the grid, then film β is deposited:

$$A^* + B^* \rightarrow \text{film } \beta\,. \tag{2}$$

In the context of the deposition discussed in this paper, A and B represent O_2 and SiH_4 (silane) reactants, respectively, and α and β, are then SiO_2 and SiO_x, respectively.

In previous publications,[5,6] we have identified the conditions under which the activation of silane can be switched on and off by the application of a particular state of grid bias. A brief description of how this is accomplished, as well as a description of the reaction chemistries for SiO_2 and SiO_x depositions is given in Sec. II. Section III discusses the sample preparation and the thin film analysis. The purpose of this paper is to emphasize the abruptness of the oxide–suboxide transition, and to study transport through the oxide layer and charge storage within the suboxide. We have prepared oxide–suboxide multilayer heterostructures and studied them by transmission electron microscopy (TEM). We have also prepared metal(M)–oxide(O)–suboxide(SO)–oxide(O)–silicon(S), (M/O/SO/O/S), devices and studied

their capacitance–voltage (C–V) characteristics as a function of the thickness of the oxide that is sandwiched between the Si and the suboxide.

II. REACTION CHEMISTRY

We have shown previously[5,6] that the deposition of silicon suboxides by remote PECVD depends on two separate reactions occurring simultaneously. The first produces an a-Si:H alloy component which introduces Si–Si and Si–H groups into the suboxide; and the second produces an SiO_2 alloy component which introduces the remaining Si–O–Si bonding groups. The deposition of a-Si:H and SiO_2 by remote PECVD are described by the following reactions:

$$\{He\}^* + SiH_4 \rightarrow a\text{-Si:H} \quad (3)$$

and

$$\{O_2 + He\}^* + SiH_4 \rightarrow SiO_2\,, \quad (4)$$

where the species within the starred brackets flow through the plasma generation region, and are plasma excited. The SiH_4 reactant is introduced downstream from the plasma excitation region. A schematic of a section of the deposition/analysis system we have used to study these particular reaction pathways, and which has also been used to deposit the films for this study, is shown in Fig. 1. This system has been previously described in detail.[5,6] A silane mixture (10% SiH_4: 90% Ar) is introduced into the deposition chamber via a gas dispersal ring downstream from the plasma generation region at a rate of 10 standard $cm^3\ min^{-1}$ (sccm). The He, or O_2 + He flow rates are set to 100 sccm and the process pressure is maintained at 300 mTorr. Under these conditions of gas flow and process pressure, the backstreaming of silane into the plasma generation region is minimized.

The key feature of this chamber relevant to this study is the plasma bias assembly, which is located immediately downstream from the plasma generation region. This consists of four electrically isolated Al plates as well as an isolated stainless steel (SS) end grid. The extent to which the plasma afterglow extends downstream from the end grid depends on the bias state of the end grid.[5] When the Al plates and the SS end grid are electrically floating, the afterglow does not extend beyond the end grid; when the grid is grounded, the afterglow extends downstream into the region of the chamber in which the silane is introduced. We have used the term *afterglow* to indicate the light emission from molecular species, which is produced mostly by impact with plasma-generated energetic electrons that are transported out of the plasma generation region. In this context, the presence of the afterglow indicates the presence of energetic electrons outside of the plasma excitation region.

For the deposition of a-Si:H, pure He gas flows into the fused silica plasma tube, and is rf excited at 13.56 MHz. Deposition of a-Si:H takes place when the end grid is grounded, i.e., when the He plasma afterglow interacts with, and activates the silane creating an excited SiH_4^* species. Studies based on mass spectrometry (MS), have demonstrated that the electron-activated silane species are not fragmented prior to the actual deposition reaction at the substrate surface.[5,6] In addition, no a-Si:H deposition occurs if

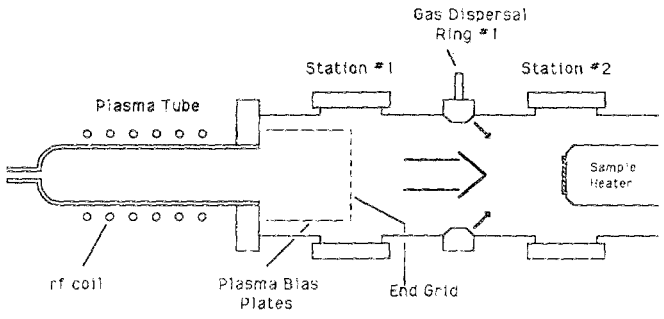

FIG. 1. Deposition/analysis chamber, showing the plasma bias plates.

the grid is in the floating state.[5,6] These results demonstrate that the function of the He discharge is to supply energetic electrons into the deposition region. We have also concluded that He metastable species, which are produced in the He plasma discharge,[6] do not play an important role in the deposition of a-Si:H because their flow through the grid assembly would not be changed by the state of the grid bias. The deposition of a-Si:H is then given the following reaction[6]:

$$e + SiH_4 \rightarrow SiH_4^* \rightarrow a\text{-Si:H(s)} + H_2(\,g) \quad (5)$$

where e represents energetic electrons injected into the plasma afterglow region.

For the deposition of SiO_2, and O_2/He mixture flows through the plasma tube and is subjected to plasma excitation. We have found[5,6] that stoichiometric SiO_2 is produced for *all* concentrations of O_2 in He investigated (from pure O_2 to as low as 0.1% O_2 in He) when the end grid is in the *floating* condition, i.e., when no afterglow extends into the deposition region. Under this condition of grid bias, the silane reactant is *not* plasma activated. With the SiH_4/Ar mixture flowing at a rate of 10 sccm, this means that the ratios of SiH_4 to O_2 which have been investigated range from 10 to 0.01, a factor of 10^3. However, the SiO_2 deposition rate increases as the O_2 flow rate is increased. This demonstrates that the deposition of SiO_2 does not involve charged species extracted from the plasma generation region, and other experiments have shown that the principal active oxygen species is neutral with the most probable species being a molecular metastable, O_2^*.[6] Equation (6) describes the deposition of SiO_2:

$$O_2^* + SiH_4 \rightarrow SiO_2(s) + H_2(g) + H_2O(g) \quad (6)$$

where O_2^* is generated when oxygen flows through the plasma tube. The relative concentrations of the by-products, $H_2(g) + H_2O(g)$, depend on the relative flow rates of $O_2 + SiH_4$, with H_2 being dominant for $O_2 < SiH_4$, and H_2O being dominant for $O_2 > SiH_4$.[5,6]

Suboxides can be deposited under the following conditions (1) the SiH_4/O_2 ratio is > 1.0,. e.g., for the 10% SiH_4/90%Ar mixture flowing at a rate of 10 sccm, the concentration of O_2 in He, flowing at 100 sccm, must be less than 1.0%, and (2) the end grid is in the grounded state so that the plasma afterglow extends beyond the grids, and the silane is excited. Note that if the grid is grounded allowing the

afterglow to extend downstream, there are two effects which can suppress the incorporation of Si–Si and Si–H bonding groups in the oxide when the O_2 concentration in He is greater than 1.0%. We find that the incorporation rate of oxygen varies linearly with the O_2 concentration for concentrations between 0.1% and 1.0%, with the 1.0% mixture producing films having O/Si ratios slightly less than 2.[5] The determining factors are the relative formation rates of the Si–Si and Si–O–Si bonding groups which result from the SiH_4^* and O_2^*, respectively. Second, it is found that as the concentration of O_2 in He increases, the intensities of the He emission lines in the discharge rapidly decrease.[6] In order to excite He atoms to emitting states, electron energies greater than about 20 eV are necessary. A decrease in the intensity of the He lines means that there are fewer energetic electrons available in which to excite these He atoms, and this in turn has an effect on the rate of generation of the SiH_4^* species that promote suboxide formation.

Although silicon suboxides are produced for SiH_4/O_2 ratios > 1.0, it is not simply a result of having too few oxygen atoms present, but also depends on the extent to which the afterglow extends beyond the plasma excitation region. In this study, we have adjusted the flow rates, plasma power, etc., so that SiO_2–SiO_x multilayer structures can be deposited by changing only one condition—the bias state of the end grid between the plasma excitation region and the deposition region. This is done without adjusting, switching, or interrupting either the gas flows or the rf power. Although we do not yet have a detailed explanation as to how the plasma bias assembly works,[5] under the floating condition, the plates and end grid float to roughly $+15$ V with respect to the potential of the chamber. This positive potential is sufficient to prevent electrons from diffusing into the chamber, and thereby contains the plasma afterglow.

Table I(A) summarizes the deposition parameters and deposition rates for the oxide and suboxide layers. The O_2 concentration is fixed to 0.2% in He by flowing a pure He source gas at 80 sccm and a 1% O_2 in He source gas at 20 sccm; this results in a SiH_4/O_2 flow ratio of about 5. The rf power is set at about 29 ± 1 W. The deposition rates were obtained[5] by measuring a step height for thick films (> 1000 Å) using a stylus instrument. For the oxides, the steps were formed by removing a small section by etching with HF acid, and for the suboxides, the steps were formed during deposition by physically masking a portion of the substrate.

III. SAMPLE PREPARATION AND PROPERTIES

A. Sample preparation

The thin film structures were deposited onto crystalline silicon substrates which were prepared by a modified RCA-clean process[7] just prior to loading into the deposition chamber. The structure which was used for the TEM analysis was deposited onto a (100) oriented p-type 30–60 Ω cm substrate. The samples prepared for the electrical measurements were deposited onto (111) oriented n-type epitaxial wafers with a resistivity of 5 Ω cm in the 15-μm thick epiregion. Aluminum dots having an area of 1.15×10^{-3} cm^2 are evaporated onto the top side of a trilayer structures through a shadow mask. Al is also evaporated onto the backside of the substrate for the contact to the $n+$ Si. After metallization, the samples were annealed at 400 °C in flowing dry N_2 for 1 h. High frequency (1 MHz) C–V measurements were carried out in the dark with a Model 410 Micromanipulator instrument. An IBM-AT computer was used to control the gate voltage (V_G) and the ramp rate, which is incremented in steps of 0.02 V; it records the capacitance data as well.

TABLE I. Deposition parameters and sample structures.

(A) Deposition conditions of silicon oxides and suboxides.

Parameters that are fixed	
% O_2 in He/flow (sccm)	0.20/100
% SiH_4 in Ar/flow (sccm)	10.0/10
SiH_4/O_2 ratio	5
rf power (W)	29 ± 1
Pressure (mTorr)	300
Temperature (°C)	300
Sample position	No. 2 station, 4.5 in. from end grid

Parameters that are varied		
End grid bias	Type of film	Deposition rate (Å/min)
Floating	SiO_2	3.6 ± 0.2
Grounded	$SiO_{1.0}$	30 ± 5

(B) SiO_2–$SiO_{1.0}$ multilayer structure for TEM measurement.

Layer	End grid bias	Type of film	Time span (min)
A	floating	SiO_2	15
B	grounded	$SiO_{1.0}$	5

(C) Samples for C–V measurements. The 1st oxide is deposited onto the c-Si substrate.

	Thickness (Å)		
Sample	1st oxide	Suboxide	2nd oxide
M04	180	...	...
M05	84	150	165
M03	40	150	165
M06	20	150	165

B. TEM measurements

One sample was prepared for the TEM analysis. A thin layer of silicon dioxide (layer A) was first deposited onto the c-Si substrate by starting with the end grid in the floating condition. Without interrupting any other deposition parameters, the grid was switched to ground and a thicker suboxide layer (layer B) was deposited. A second oxide layer was then initiated by switching the grid again back to the floating condition. This sequence was then repeated until five "A,B" pairs were deposited with a final oxide capping the multilayer structure. The deposition times for these layers are given in Table I(B).

Figure 2 shows the cross-sectional bright-field TEM image taken on a Hitachi H-800 instrument using 200 keV primary electrons at a magnification of 100 K. The atomically

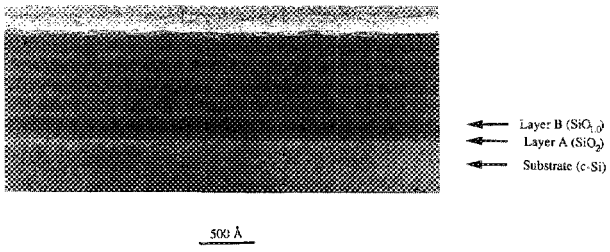

FIG. 2. TEM of multilayer structure. Layer A is SiO_2 and layer B is $SiO_{1.0}$.

denser suboxide layers show up in the micrograph as the dark bands, whereas the lighter bands are the oxide layers. The first order layer is about 79-Å thick, and the subsequent oxides are all slightly thinner, approximately 52-Å thick. The suboxide layers are all about 145-Å thick. We estimate the error in the thickness determinations to be around 13 Å. We conclude further from this micrograph that the suboxide material is an homogeneous alloy of Si and O, and is not a diphasic mixture of *a*-Si and *a*-SiO_2. Finally, the micrograph demonstrates that the metallurgical interface between the oxide and suboxide layers is less than 15 Å. We are currently studying the factors that contribute to the uncertainty in this determination.

C. *C–V* measurements

Several different samples were prepared for *C–V* measurements. A description of these structures is presented in Table I(C). Sample M04 consists of a single layer (of oxide) in a metal–oxide semiconductor (MOS) configuration. This sample serves as a benchmark for evaluating the electrical quality of the deposited oxide layers. The *C–V* data for this sample is shown in Fig. 3, where the trace from + 5 to − 5 V, and the retrace are approximately overlapping. The scan speed is 10 V/s and a delay period of 1 ms occurs before beginning the retrace. Scans taken after this show that the curves shift in the negative voltage direction, indicating a buildup of positive oxide charge, possibly from mobile ions originating at the oxide-gate interface.

To investigate the potential for charge storage in the suboxides, three samples were made, each consisting of three layers. A thin oxide layer was first deposited onto the *c*-Si substrate, followed by a suboxide layer, followed finally by a thicker oxide. Only the thickness of the first oxide layer was varied [see Table I(C)]; the thickness of the suboxide layer and of the second oxide layer were fixed at approximate 150 and 165 Å, respectively. The thickness of the first oxide layer is varied in order to control tunnel injection from the Si substrate into the suboxide, and from the suboxide back into the Si substrate. In contrast, the second oxide layer is sufficiently thick to prevent any tunneling from either the suboxide to the metal gate or in the reverse direction.

The *C–V* data for samples M05, M03, and M06, are shown in Figs. 4–6, respectively. The *C–V* curves for sample M05 (Fig. 4) are similar to those of M04 (Fig. 3) in that the

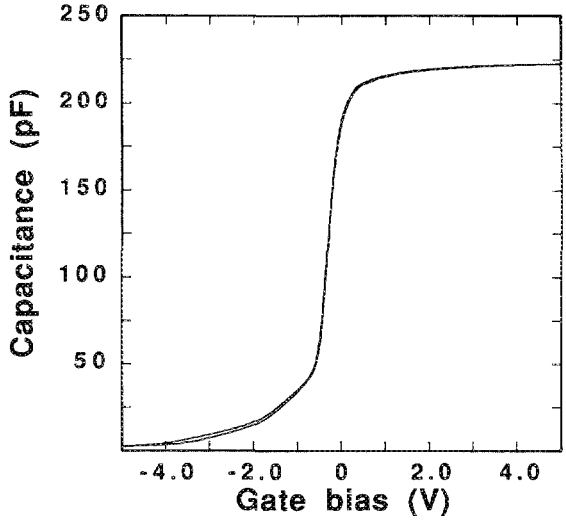

FIG. 3. *C–V* curves of sample M04 [see Table I(C)]. The scan speed is 10 V/s and the delay time between the trace and the retrace curves is 1 ms.

curves have not shifted toward a positive gate voltage; this indicates that little or no injection of electrons from the substrate into the suboxide layer has occurred. This is expected because of the relatively thick oxide barrier ($\sim$84 Å).

For the samples having thinner oxide layers, the *C–V* data (Figs. 5 and 6) show that negative charge can tunnel into the suboxide layer as evidenced by the positive shift ($\sim$ + 4 V) in the flat-band voltage of the initial traces. Before initiating a trace, the gate voltage (V_G) was held at + 5 V for a period of time on the order of $\sim$5 min. This was to ensure that the amount of negative charge has tunneled into the suboxide is the same before each scan is made. This is indeed the case as evidenced by the flat-band shifts of just under 4 V for all of the initial traces in Figs. 5 and 6.

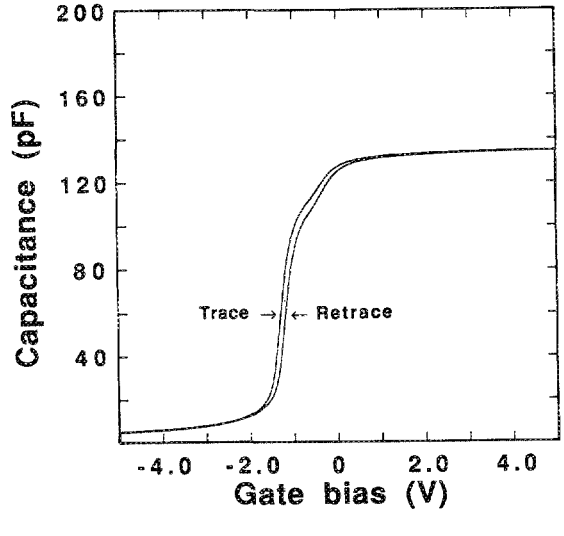

FIG. 4. *C–V* curves of sample M05 [see Table I(C)]. The scan parameters are the same as those in Fig. 3.

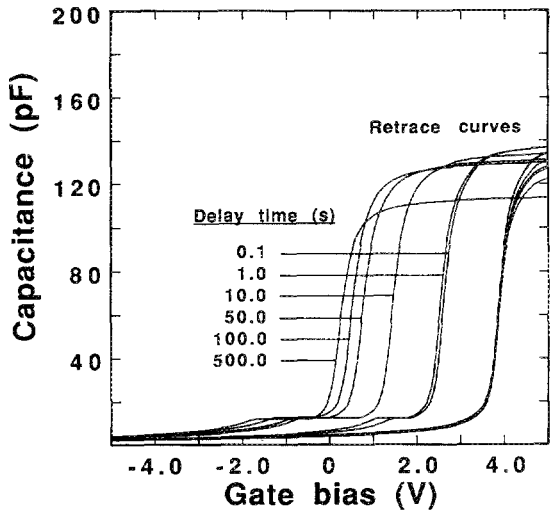

FIG. 5. *C–V* curves of sample M03 [see Table I(C)]. The scan speed is 10 V/s and the delay time between the trace and retrace curves varied between 0.1 and 500 s.

As V_G swings negative during the initial trace, electrons can tunnel back out of the suboxide into the silicon substrate. It is evident that the shape of the *C–V* curves depends on the scan sweep rate and the ability of the charge to tunnel back out of the suboxide at a given V_G. Rather than show the effects of different scan speeds, Figs. 5 and 6 show the effect of different delay periods between the end of the trace and the beginning of the retrace. We therefore investigate the time dependence of the discharging mechanism by maintaining a V_G of -5 V at the end of the trace for different time delays. The scan speeds for the trace and retrace curves are the same as before, 10 V/s. With this scan speed, discharging

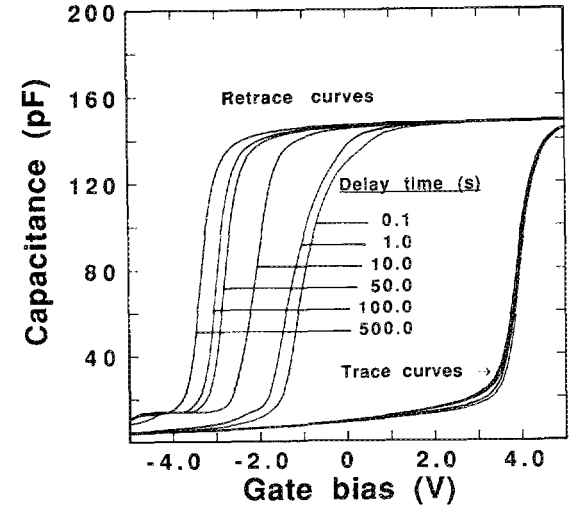

FIG. 6. *C–V* curves of sample M06 [see Table I(C)]. The scan speed is 10 V/s and the delay time between the trace and retrace curves varied between 0.1 and 500 s.

effects requiring times longer than about 1 s can be investigated.

As the delay time increases from 0.1 to 500 s for sample M03 (oxide thickness = 40 Å), the retrace curves are displaced in the negative voltage direction with the flat-band voltage approaching 0 V as the delay time increases toward 500 s. For shorter delay times, the flat-band voltages are more positive, and they decrease in magnitude with increasing delay time. This behavior indicates that most of the electrons have tunneled back out of the suboxide layer into the Si substrate during the 500 s delay period at which the gate voltage was held at -5 V. In contrast to sample M03, even a time delay of as small as 0.1 s for sample M06 (oxide thickness = 20 Å) is sufficient for all of the electrons to leave the suboxide layer, and for the suboxide layer to take on a net positive charge as evidenced by the negative flat-band shift.

D. Analysis of the *C–V* data

The *C–V* data can be used to estimate a low frequency dielectric constant for the suboxide material. Figures 5 and 6 show that the maximum capacitance of samples M03 and M06 is about 135 and 149 pF, respectively. If the difference between these values is due to the difference in the thickness of the first oxide layer, then we estimate that the dielectric constant for the suboxide between 6.6 and 7.2. Values in this range are expected since they must fall between the values for silicon and silicon dioxide, 11.7 and 3.9, respectively. As the O/Si ratio increases from zero, we expect[8] that the optical band gap (E_G) should increase.[8] We have measured E_G for suboxides[9] as defined by the E04 value, i.e., the E04 is photon energy at which the absorption constant is 10^4 cm^{-1}. For suboxides having an O/Si ratio ≈ 1.0, we find that E_G is about 2 eV, consistent with previously reported data for homogeneous suboxides.[10]

The *C–V* data can also be used to study charging effects.[11] In this case, we are interested in the charge which has tunneled into the suboxide layer of the M/O/OS/O/S structure and has become trapped. Both of the trace scans for samples M03 and M06 show the same positive shift ($\sim +4$ V) in the *C–V* curve indicating that with the application of the $+5$ V gate bias, about 3×10^{12} electrons/cm^2 have tunneled out of the Si substrate, through the first oxide, and into the suboxide layer where they have become trapped before the trace scan was initiated.

The data presented in Figs. 5 and 6 allow us to investigate the time dependence of the discharge process. This is accomplished by sweeping rapidly from a V_G of $+5$ V to a V_G of -5 V during the trace scan, and then delaying for a period of time before retracing rapidly back to a V_G of $+5$ V. By increasing the delay time for the negative bias, the number of electrons extracted from the suboxide can increase. In this experiment, the change of the flat-band voltage, ΔV_{FB}, of the retrace can be used to monitor the amount of charge remaining in the suboxide after a time-dependent partial discharge. Figure 7 shows the results of this analysis for samples M03 and M06, where we plot the voltage at which the capacitance has risen to an arbitrarily chosen value of 80 pF vs the delay time; this voltage is denoted as $V(C = 80\,\text{pF})$. We have used $V(C = 80$ pf) rather than ΔV_{FB} because it is more easily

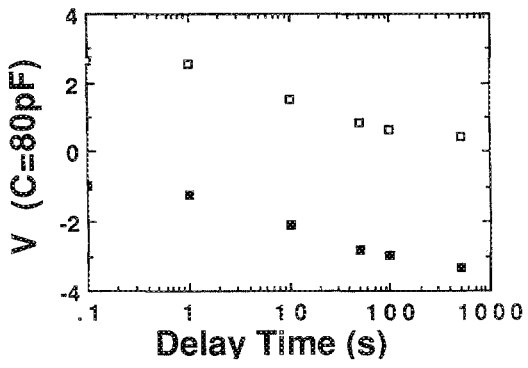

FIG. 7. Plot of discharging vs delay time at a V_G of 5 V for samples M03 (□) and M06 (■). The charge remaining in the suboxide is proportional to the voltage shift in the C–V curves. Here, we choose the voltage of the retrace curve at which the capacitance has risen to a level of 80 pF.

determined from the C–V plots and because it provides a measure relative discharging rates.

There are four things to note in Fig. 7. First, the time required to completely discharge the suboxide at a V_G of -5 V for sample M03, which has an oxide thickness of 40 Å, is on the order of more than 1000 s. Second, by decreasing the barrier thickness by a factor of one half (sample M06) the sample completely discharges in a time of less than 0.1 s. Third, as the delay time increases beyond 0.1 s, sample M06 becomes positively charged as indicated by the negative values of $V(C = 80\ \text{pF})$. And last, the trends in the data for the two oxide thicknesses are the same with increasing delay time.

IV. DISCUSSION

In earlier work, we have stated that one of the principal advantages of remote PECVD over direct PECVD[12] is the ability to control the stoichiometry of the film by reducing the variety of chemically active species created. This is accomplished by selectively exciting the reactant gases. In particular, by preventing the excitation of silane, either by preventing silane from back streaming into the plasma generation region or by eliminating the plasma after glow from the deposition region, stoichiometric films of SiO_2 can be produced. We then showed[5] that the deposition of silicon suboxides by remote PECVD required, in addition to the excitation of oxygen, the excitation of silane. We showed further[5] that the excitation of silane was accomplished by its interaction with the plasma afterglow, and that the extension of the afterglow into the deposition chamber could be controlled with the selectivity biasing of a grid assembly between the plasma excitation region and the deposition region. In this way, the ability to either activate only O_2 or both O_2 and SiH_4 allows one to switch between depositing either SiO_2 or SiO_x films; the SiH_4/O_2 flow ratios determine the suboxide composition, x. Infrared studies[13] have shown that a value of x equal to 1 can be achieved with a SiH_4/O_2 ratio of about 5. In this paper, we have demonstrated the ability to produce multilayer $SiO_2/SiO_{1.0}$ heterostructures by varying only the bias of the grid structure.

Suboxides produced from high temperature chemical vapor deposition (CVD) processes[14,15] are generally diphasic mixtures of SiO_2 and Si. Infrared studies of the suboxides produced by remote PECVD[13] support the work by H. R. Philipp[10] showing that the plasma deposited suboxides are homogeneous alloys. The TEM image shown in Fig. 2 supports this picture by showing that if inhomogeneities do exist in the suboxide, they are no more than 15 Å in extent.

The MOS characteristics of silicon dioxide films produced by remote PECVD have been extensively investigated by our colleagues at the Research Triangle Institute[16,17] and by our group as well.[7] It is found that silicon dioxide can be deposited on c-Si substrates with a very low density of interfacial defects, on the order of 3×10^{10} cm^{-2} eV^{-1} or less, for oxides deposited at temperatures about 200 °C. Above this temperature however, the quality of the interface deteriorates. This degradation has been attributed to a subcutaneous oxidation process,[17,7] in which the silicon substrate is oxidized during the deposition process. The multilayer structure studied by TEM shows evidence for this subcutaneous process. This is expected to become an important factor for oxides deposited at temperatures of 300 °C. In spite of the fact that the deposition times for all the oxides were the same, 15 min, the first oxide layer, which was deposited directly onto the c-Si substrate, is approximately 30 Å thicker than the subsequent oxide layers. If this enhancement is in fact due to the subcutaneous oxidation process, this TEM image then suggests, that any subcutaneous oxidation of the suboxide layers proceeds at a significantly reduced rate.

Finally, we have investigated the charge storage capability of M/O/OS/O/S structures for applications in memory device structures. The three requirements any structure must satisfy for such applications include: (1) charge injection into a storage layer; (2) charge trapping in the storage layer; and (3) charge removal from the storage layer. For the structures we investigated, the suboxide layer provides charge storage, and the oxide layers can prevent the trapped charge from escaping back to the semiconductor substrate or the gate electrode. The charge injection and removal are both accomplished by direct tunneling. With the application of + 5 V to the gate, electric fields across the oxide layers are less than about 3 MV/cm, and so the injection is by direct tunneling, rather than by Fowler–Nordheim tunneling, or by any breakdown process. The 84-Å thick oxide did not allow electrons to tunnel into the suboxide layer, whereas the 20-Å thick barrier, allowed tunneling into the suboxide and did not prevent the suboxide from discharging. The 40-Å thick barrier satisfied both of these requirements, allowing tunnel injection but preventing discharging. Complete charge removal through the 40 Å oxide could be accomplished by applying a -5 V gate bias for a period of time of more than 1000 s.

Although samples M03 and M06 charge negatively with the application of positive gate bias potential, only sample M06 could be charged positively when the opposite potential is applied to the gate. For sample M03, only electrons corresponding to the original number injected into the suboxide

layer could be removed. For sample M06, all of these electrons are easily removed, and in addition, if the gate is held at -5 V for periods of time longer than a few seconds, the suboxide becomes positively charged. Either holes from the substrate are tunneling into the suboxide, or electrons in the suboxide are tunneling back into the substrate. Positively charged suboxides have also been observed by other workers[15] and they are thought to be associated with the removal of electrons originating in donor-like states in the suboxide, and not from hole injection.

ACKNOWLEDGMENTS

This research is supported by ONR, SRC, SEMATECH, and the NSF Engineering Research Center for Advanced Electronic Materials Processing.

[1]B. Abeles and T. Tiedje, in *Semiconductors and Semimetals*, edited by J. I. Pankove (Academic, New York, 1984), Vol. 21, part C, p. 407.
[2]S. C. Agarwal and S. Guha, Phys. Rev. B **31**, 5547 (1985).
[3]K. Hattori, M. Tsujishita, H. Okamoto, and Y. Hamakawa, Appl. Phys. Lett. **55**, 763 (1989).
[4]P. D. Richard, R. J. Markunas, G. Lucovsky, G. G. Fountain, A. N. Mansour, and D. V. Tsu, J. Vac. Sci. Technol. A **3**, 867 (1985).
[5]D. V. Tsu, G. Lucovsky and M. W. Watkins, in *Chemical Perspectives of Microelectronic Materials*, edited by M. E. Gross, J. M. Jasinski, and J. T. Yates, Jr. (to be published).
[6]D. V. Tsu, G. N. Parsons, G. Lucovsky, and M. W. Watkins, J. Vac. Sci. Technol. A **7**, 1115 (1989).
[7]S. S. Kim, D. J. Stephens, G. Lucovsky, G. G. Fountain, and R. J. Markunas, J. Vac. Sci. Technol. A **8**, 2039 (1990).
[8]T. S. Moss, *Optical Properties of Semi-Conductors*, (Butterworths, London, 1959), p. 48.
[9]G. N. Parson (private communication).
[10]H. R. Philipp, J. Non-Cryst. Solids **8–10**, 627 (1972).
[11]E. H. Nicollian and J. R. Brews, *MOS (Metal Oxide Semiconductor Physics and Technology*, (Wiley, New York, 1982).
[12]G. Lucovsky and D. V. Tus, J. Non-Cryst. Solids **97&98**, 265 (1987).
[13]D. V. Tsu, G. Lucovsky, and B. N. Davidson, Phys. Rev. B **40**, 1795 (1989).
[14]D. J. DiMaria and D. W. Dong, J. Appl. Phys. **51**, 2722 (1980).
[15]M. Lopez and C. Falcony, J. Mater. Res. **4**, 1233 (1989).
[16]G. G. Fountain, R. A. Rudder, S. V. Hattangady, R. J. Markunas, and P. S. Lindorme, J. Appl. Phys. **63**, 4744 (1988).
[17]G. G. Fountain, S. V. Hattangady, R. A. Rudder, R. J. Markunas, G. Lucovsky, S. S. Kim, and D. V. Tsu, J. Vac. Technol. A **7**, 576 (1989).